

Towards a free-free template for CMB foregrounds

C. Dickinson,^{1*} R. D. Davies,¹ and R. J. Davis¹

¹*Jodrell Bank Observatory, Dept of Physics & Astronomy, University of Manchester, Macclesfield, Cheshire SK11 9DL UK.*

Received ****insert****; Accepted 21st January, 2003

ABSTRACT

A full-sky template map of the Galactic free-free foreground emission component is increasingly important for high sensitivity CMB experiments. We use the recently published $H\alpha$ data of both the northern and southern skies as the basis for such a template.

The first step is to correct the $H\alpha$ maps for dust absorption using the $100\ \mu\text{m}$ dust maps of Schlegel, Finkbeiner & Davis (1998). We show that for a range of longitudes, the Galactic latitude distribution of absorption suggests that it is 33 per cent of the full extragalactic absorption. A reliable absorption-corrected $H\alpha$ map can be produced for ~ 95 per cent of the sky; the area for which a template cannot be recovered is the Galactic plane area $|b| < 5^\circ$, $l = 260^\circ - 0^\circ - 160^\circ$ and some isolated dense dust clouds at intermediate latitudes.

The second step is to convert the dust-corrected $H\alpha$ data into a predicted radio surface brightness. The free-free emission formula is revised to give an accurate expression (1 per cent) for the radio emission covering the frequency range 100 MHz to 100 GHz and the electron temperature range 3000 to 20000 K. The main uncertainty when applying this expression is the variation of electron temperature across the sky. The emission formula is verified in several extended HII regions using data in the range 408 to 2326 MHz.

A full-sky free-free template map is presented at 30 GHz; the scaling to other frequencies is given. The Haslam et al. all-sky 408 MHz map of the sky can be corrected for this free-free component, which amounts to a ≈ 6 per cent correction at intermediate and high latitudes, to provide a pure synchrotron all-sky template. The implications for CMB experiments are discussed.

Key words: cosmic microwave background - radio continuum: ISM - dust, extinction - HII regions - radiation mechanisms: thermal

1 INTRODUCTION

Current CMB experiments are sensitive enough to measure the primordial fluctuations which have an amplitude in the range of $\approx 20 - 100\ \mu\text{K}$ over the ℓ -range $10 - 2000$ which corresponds to angular scales of $\approx 10^\circ - 10$ arcmin (Hanany et al. 2000; Mauskopf et al. 2000; Padin et al. 2001; Halverson et al. 2002; Scott et al. 2002). The angular power spectrum of these fluctuations contains a wealth of cosmological information. One of the crucial factors in determining an accurate power spectrum of these fluctuations is understanding and removing the foreground contamination. The amplitude of the foreground signal depends on frequency, angular scale and region of sky being observed. CMB foregrounds comprise point sources and diffuse Galactic foregrounds. Point

sources are a particular problem at smaller angular scales ($\lesssim 30$ arcmin), while diffuse foreground structures become dominant on larger angular scales. Here we concentrate on the problem of diffuse Galactic foregrounds at frequencies below < 100 GHz, a frequency range which is used in current and upcoming CMB experiments such as the *MAP* and *Planck* satellites.

1.1 Galactic foregrounds

The diffuse Galactic foreground has 3 (possibly 4) components. i) *Synchrotron* emission from relativistic electrons spiralling in the Galactic magnetic field dominates at frequencies below 1 GHz with a spectral index ($T \propto \nu^{-\beta}$) of $\beta \approx 2.7 - 3.2$ (Davies et al. 1996). It is traced by low-frequency surveys such as those of Haslam et al. (1982), Reich & Reich. (1988) and Jonas et al. (1998) where it is

* E-mail: cdickins@jb.man.ac.uk

seen to extend well above the plane - e.g. the North Polar Spur which extends to Galactic latitude $b \approx 80^\circ$. ii) *Free-free* bremsstrahlung emission from thermal electrons has a flatter spectral index of $\beta \approx 2.1$. It is the dominant foreground at frequencies between $\nu = 10 - 100$ GHz, where microwave CMB experiments operate (e.g. DASI, CBI, VSA, *MAP*, *Planck*). The optical $H\alpha$ line is a good tracer of free-free emission although it requires corrections for dust absorption. iii) The *vibrational* emission from thermal dust is dominant at frequencies above ~ 100 GHz. This is thermal emission from warm dust and is well-traced at $\lambda \sim 100 \mu\text{m}$ where it has its peak. iv) An *anomalous* component has recently been discovered (Kogut et al. 1996; Leitch et al. 1997; de Oliveira-Costa et al. 1997,1998,1999,2000,2002; Finkbeiner et al. 2002). Draine & Lazarian (1998) proposed that this could be due to *spinning* dust grains emitting in a 1-2 octave band centred at ~ 20 GHz. It was first believed to be due to free-free emission (Kogut 1996), but this has been ruled out primarily by the lack of associated $H\alpha$ emission.

The separation and quantifying of the individual CMB foreground components is a continuing challenge. Each component is of interest in its own right; its angular distribution and spectrum are basic parameters. They all contribute as foregrounds to the CMB and their removal is necessary to realize the full potential of current high sensitivity CMB surveys where C_l values are to be measured to an accuracy of a few percent. Such separations are best made using templates for each component. With the advent of the $H\alpha$ survey, such a template is now available for each of the 4 proposed components. Although some approaches to separation of components are being made which reduce the assumptions about the template parameters (e.g. Baccigalupi et al. 2000; Vielva et al. 2001) they still face difficulties where the components are correlated. For example all the foregrounds are quasi-correlated as they increase strongly towards the Galactic plane. Also, the $H\alpha$ and (spinning) dust emissions show considerable correlation over most of the sky (see Section 7); this was at the root of the original misunderstanding of the anomalous component. If one has a good free-free template as we derive here, the other 3 foreground components can be well-characterized except possibly at the lowest Galactic latitudes.

1.2 Large-area $H\alpha$ surveys

Extensive filamentary $H\alpha$ emission regions, of galactic origin, were first found by Meaburn (1965, 1967) extending to high Galactic latitudes; Sivan (1974) demonstrated the wealth of $H\alpha$ emission at low-intermediate latitudes but at a relatively low sensitivity of $\approx 15 R$; we note that $1 \text{ Rayleigh } (R) \equiv 10^6/4\pi \text{ photons s}^{-1} \text{ cm}^{-2} \text{ sr}^{-1} \equiv 2.41 \times 10^7 \text{ erg s}^{-1} \text{ cm}^{-2} \text{ sr}^{-1} \equiv 2.25 \text{ cm}^{-6} \text{ pc}$ for $T_e = 8000 \text{ K}$ gas. Several large and very sensitive $H\alpha$ surveys are now well under way. The most relevant surveys are listed in Table 1. In the northern sky covering declinations $\delta \gtrsim -30^\circ$ the Wisconsin H Alpha Mapper project (WHAM) is the most sensitive $H\alpha$ survey to-date, but is restricted to an angular resolution of $\approx 1^\circ$ (Reynolds et al. 1998; Haffner 1999). The final sensitivity in each field is $\approx 0.05 R$ and the data are calibrated to an accuracy conservatively estimated at 10 per cent. WHAM is a dual etalon Fabry-Perot spectrometer with a velocity resolution of 12 km s^{-1} . The spectra can be used to remove the

geocoronal $H\alpha$ emission from the Earth's upper atmosphere which varies in strength from 2-13 R ; it is much brighter than the Galactic signals at high Galactic latitudes.

The ongoing Virginia Tech Spectral-line Survey (VTSS) is a complimentary narrow-band imaging survey of the northern sky covering $\delta \gtrsim -15^\circ$ (Dennison, Simonetti & Topsana 1998). It has a resolution of 1.6 arcmin in each 10° diameter field, which will be good enough for almost all CMB experiments as most of the cosmological information is contained on scales between $10^\circ - 10$ arcmin. However, on larger angular scales, it will most likely be limited by the geocoronal emission which appears as a time-varying background signal of unknown level. Star residuals which have not been subtracted correctly can also be a problem. In combination with the WHAM survey, this survey will be a powerful tool.

The recently published (Gaustad et al. 2001) Southern H Alpha Sky Survey Atlas (SHASSA) covers the southern sky $\delta \leq +15^\circ$ at an angular resolution of 0.8 arcmin in each 13° field. The sensitivity reaches 2 R limited by geocoronal emission and star residuals which have been partially removed by median filtering. Smoothing this survey to a resolution of 4 arcmin allows features of about 0.5 R to be detected. The intensity calibration is accurate to about 9 per cent.

Two other $H\alpha$ surveys are in progress. The Manchester Wide-Field Camera (MWFC) can observe $H\alpha$ with a 32° field of view with 7 arcmin resolution (e.g. Boumis et al. 2001) and a sensitivity of $\approx 1 R$. This instrument is particularly sensitive to large scale features ($\gtrsim 1^\circ$) which may be missed by cameras with smaller fields. We have recently observed several selected fields to look for diffuse $H\alpha$ emission, both in the northern and southern hemispheres. The AAO/UK Schmidt $H\alpha$ survey has high angular resolution (1 arcsec) but is restricted to the Galactic plane at relatively low sensitivity (Parker & Phillips 1998) as given in Table 1.

1.3 This paper

In this paper we describe the steps taken to derive a free-free emission template from recently published $H\alpha$ surveys. In Section 2 we determine the absorption of the Galactic $H\alpha$ emission by dust based on the $100 \mu\text{m}$ dust template given by Schlegel, Finkbeiner & Davis (1998), hereafter SFD98; a statistical estimate is made of the relative distribution of the $H\alpha$ emission and the dust in the line of sight. Section 3 summarizes the expressions required to convert the dust-corrected $H\alpha$ emission into microwave emission at frequencies relevant to current CMB experiments. The uncertainties in the relation are evaluated. This relationship is tested in Section 4 using available radio surveys. The final free-free template is presented in Section 5. The 408 MHz all-sky map of Haslam et al. (1982) corrected for free-free emission is derived in Section 6; it is the best available synchrotron template. We discuss the implications of the new template for upcoming CMB experiments and for interstellar medium (ISM) studies in Section 7. The final conclusions of this work are given in Section 8.

Table 1. Current H α surveys relevant to CMB observations

Survey	Type	Field of View (degrees)	Resolution (arcmin)	Sensitivity/pixel (R)	Sky coverage
WHAM	Fabry-Perot Spectroscopy	1	60	≈ 0.05	$\delta \geq -30^\circ$
VTSS	Narrow-band Imaging	10	1.6	≈ 1	$\delta \geq -15^\circ$
SHASSA	Narrow-band Imaging	13.6	0.8	≈ 2	$\delta \leq +15^\circ$
MWFC	Narrow-band Imaging	32	7	≈ 1	Selected fields
AAO/ Schmidt	Narrow-band Imaging	5.5	0.02	$\approx 5 - 10$	$ b \leq 10^\circ$

2 CORRECTION OF H α FOR DUST ABSORPTION

2.1 The Galactic distribution of absorption

It is clear that the use of H α surveys as a template for free-free emission will be jeopardized in the Galactic plane where visual absorption is typically 1 magnitude per kiloparsec in the local arms and where the total absorption to the Galactic centre is ≈ 20 magnitudes. At intermediate latitudes the absorption broadly follows a cosecant law with a vertical slab half-thickness of 0.1 to 0.2 blue magnitudes. Such a cosecant law was widely used in extragalactic astronomy. In order to take account of the known structure in the obscuration, the line integral of HI combined with a factor derived from the Shane-Wirtanen galaxy counts was introduced by Burstein & Heiles (1978). This procedure took account of the possibility that the gas-to-dust ratio might not be constant and the fact that not all hydrogen is in the neutral atomic form. The Burstein-Heiles approach is limited by the angular resolution of HI all-sky surveys which is currently ~ 30 arcmin.

A new approach which provides a resolution of 6.1 arcmin and has a complete all-sky coverage is offered by SFD98 who use far infra-red data from the *COBE-DIRBE* and *IRAS* satellites. This combination of data at a range of FIR wavelengths enabled a good zero level to be established, an adequate removal of zodiacal light and a more effective destripping than previously. Also, by comparing the *DIRBE* 240 μm and *IRAS* 100 μm to derive a dust temperature, an estimate could be made of the dust column density, D^T , measured in units of MJy sr^{-1} , in terms of a 100 μm surface brightness at a fixed temperature of 18.2 K. This correction to a fixed temperature can only be made on the angular scale of the *DIRBE* observations, namely $0^\circ.7$, and consequently is not strictly true on the 6.1 arcmin scale of the D^T dust maps. The dust temperatures are typically in the range 17 – 21 K which corresponds to a correction of up to a factor of ~ 5 in the dust column density (see SFD98).

2.2 Derivation of a H α absorption template

We will adopt the D^T dust template as the indicator of dust absorption. This then requires a conversion factor to

estimate the absorption at 656.3 nm, the H α wavelength. SFD98 use the $(B-V)$ colours of some 470 galaxies at a wide range of Galactic coordinates to derive a best fit correlation with the D^T value at the position of each galaxy. They find the $E(B-V)$ colour can be estimated from D^T with the expression $E(B-V) = (0.0184 \pm 0.0014)D^T$ magnitudes and claim that the reddening estimated in this way has a standard deviation of 16 per cent at any given position.

In order to estimate the absorption at the H α wavelength we use the parametric extinction curve for optical wavelengths given by O'Donnell (1994) and find the Galactic absorption at H α to be $A(\text{H}\alpha) = 0.81A(V)$. Assuming the dust is characterized by a reddening value $R_V = A(V)/E(B-V) = 3.1$, this leads to an absorption at H α of

$$A(\text{H}\alpha) = 2.51E(B-V) = (0.0462 \pm 0.0035)D^T \text{ mag} \quad (1)$$

where D^T is in units MJy sr^{-1} . The values given in table 6 of SFD98 are 6 per cent higher than this, corresponding to a higher value of R_V .

A range of reddening laws, characterized by different values of R_V , are found in different directions in the Galaxy. The different laws are thought to derive from different grain chemistry and size distributions. Values of R_V range from 2.5 to 5, with the higher values often in denser dust clouds. A value of 3.1 is widely adopted as representative of the diffuse ISM in directions away from dense dust clouds. However, it should be emphasized that this is only an average value and that any line of sight will have a scatter about this value. Putting all these statistical factors together we consider that the relationship between $A(\text{H}\alpha)$ and D^T is accurate to about 20 per cent.

2.3 The absorption of Galactic H α

The expression given in the preceding section applies to absorption of extragalactic objects at optical wavelengths. Here we are considering Galactic H α emission which is mixed with the dust. At first sight it might be argued that since the dust and gas are uniformly mixed, then the ionized gas and the dust would also be uniformly mixed. The correlation between gas and dust will be discussed further in Section 7.

The major part of the H α seen from our position in the Galaxy is the result of ionization by the UV radiation field from young stars embedded in the dust plus the contribution from nearby regions of localized recent star formation. Such regions include the Gould Belt system which reaches to Galactic latitudes of 40° or more.

We seek a first-order absorption formula for correction of the H α emission based on the dust distribution given by SFD98. If the ionized gas were uniformly mixed with the dust then the average absorption would be half the extragalactic value given in Section 2.2 on the assumption that the dust absorption is optically thin (say ≤ 0.5 mag). We define f_d , the effective dust fraction in the line of sight actually absorbing the H α so that the actual absorption of H α is given by $f_d \times A(\text{H}\alpha)$, where $A(\text{H}\alpha)$ is the full extragalactic absorption. For example, uniformly mixing of ionized gas and dust corresponds to $f_d = 0.5$. There would be a systematic modification of this value if the z-distribution of the dust and the ionized gas were not the same. An example would be the ionization produced by the interstellar radiation field propagating away from the plane and ionizing the “under”-side of the gas clouds which were themselves optically thick to the UV ionizing radiation. This would lead to a narrower z-distribution of H α emission than dust, which is assumed to be well-mixed with the gas, and to a reduced value of f_d .

We are now in the position to test the uniform mixing hypothesis by comparing at low and intermediate latitudes the z-distribution of neutral gas (HI), ionized gas (H α) and dust.

2.4 Galactic latitude scans

By plotting the H α dependence on Galactic latitude b , and comparing this with the unabsorbed gas indicators of HI and FIR dust (D^T), we can estimate the H α absorption as a function of b and determine a best-fitting value of f_d , the effective dust fraction producing absorption.

For neutral HI gas we use the 1420 MHz Leiden-Dwingeloo northern sky survey (Hartmann & Burton 1997), H α data from the WHAM survey and the SFD98 100 μm D^T map to trace the dust. Each map was resampled onto a Galactic coordinate grid and smoothed to a resolution of 1°. Along each 1°-wide latitude strip, the values are averaged over a range of longitudes to give a representative value for that latitude. Fig. 1 shows the latitude dependence of the gas and dust in the region $l = 30^\circ - 60^\circ$. Both the HI gas and 100 μm dust follow similar cosecant-law trends. Assuming a homogeneous slab of material viewed at different latitudes b , the column density along a line of sight is expected to follow a cosecant law when viewed from the central plane;

$$I = A_0 + A_1/\sin(|b|) \quad (2)$$

where A_0 is an offset and A_1 is the amplitude of the cosecant law. This is indeed found to be the case, with deviations occurring due to large concentrations of emitting material such as extended HII regions and features like the Local System (Gould Belt). The region $l = 30^\circ - 60^\circ$ is one of the “cleaner” regions of the plane where no large structures exist. This region includes our own spiral arm and the Sagittarius arm; here the dust emission on the Galactic ridge reaches an average of 500 MJy sr $^{-1}$ corresponding to $A(\text{H}\alpha) = 23$ mag for

an extragalactic object. At intermediate and high latitudes ($|b| > 15^\circ$), D^T is $\lesssim 8$ MJy sr $^{-1}$ and the H α absorption is therefore small.

The best-fitting cosecant law is a good match to the HI and dust distributions as shown in Fig. 1. This figure also shows that the H α intensity is greatly attenuated at low latitudes ($|b| < 15^\circ$) due to the increased dust absorption nearer to the plane. Note also that there is a significant offset A_0 ; this corresponds to the Sun being in a local “hole”. The A_0/A_1 values suggests that there is a $\sim 30 - 50$ per cent deficit in the local slab density. If one adopts equation (1) as the model for H α absorption we can correct the H α emission, adopting a value of f_d as discussed in Section 2.3. We can then determine a value for f_d by correcting the H α latitude distribution for absorption, so that it matches that of the gas and dust distributions shown in Fig 1. By varying f_d we find the best-fitting value is given by $f_d = 0.33^{+0.10}_{-0.15}$. The fit was made by deriving the cosecant law using data at $|b| > 20^\circ$ and fitting f_d to this cosecant law over $|b| = 5^\circ$ to 15° . For $|b| < 5^\circ$, the absorption is likely to be > 1 mag and therefore any derived value for f_d becomes unreliable. The value $f_d = 0.33$ derived here is representative of the solar neighbourhood of our Galaxy within a few kilo-parsecs. Other longitudes gave similar results, although the cosecant fitting is difficult due to local structures such as the Gould Belt system and other bright extended HII regions. Further information on the value of f_d is obtained from the study of the radio free-free emission from several nearby HII complexes given in Section 4.

The value of f_d derived in this section is not consistent with uniform mixing of ionized gas and dust which requires $f_d = 0.5$. However, there is a large uncertainty in f_d and it is expected that f_d will vary significantly across the sky. However, as a first-order approach, we will adopt the value $f_d = 0.33$ when estimating the free-free template in Section 5. This lower value is indicative of non-uniform ionization; for example, a region of cloud is ionized by the interstellar radiation field which is in a narrower Galactic layer of O,B stars.

2.5 The H α absorption template

Using equation (1) we can convert the D^T dust map to an absorption map which can be applied to the H α intensity $I_{\text{H}\alpha}$, using

$$I_{\text{H}\alpha}^{\text{corrected}} = I_{\text{H}\alpha} \times 10^{D^T \times 0.0185 \times f_d} \quad (3)$$

The value of f_d is taken to be 0.33. The absorption template to be applied to Galactic H α and smoothed to a resolution of 1° is shown in Fig. 2.

The template clearly shows that the absorption of H α by dust is modest - less than 0.2 mag (20 per cent correction) for most of the sky. Beyond $|b| \gtrsim 50^\circ$, it is less than 0.05 mag (5 per cent correction). At $|b| \lesssim 5^\circ$, the absorption increases beyond 1 mag for much of the Galactic plane. Individual dust clouds can have > 1 mag of absorption at intermediate latitudes. For a major portion of the sky the dust correction clearly needs to be taken into account. For example, the correction of more than 50 per cent is required in a limited area of the sky such as the Gould Belt system.

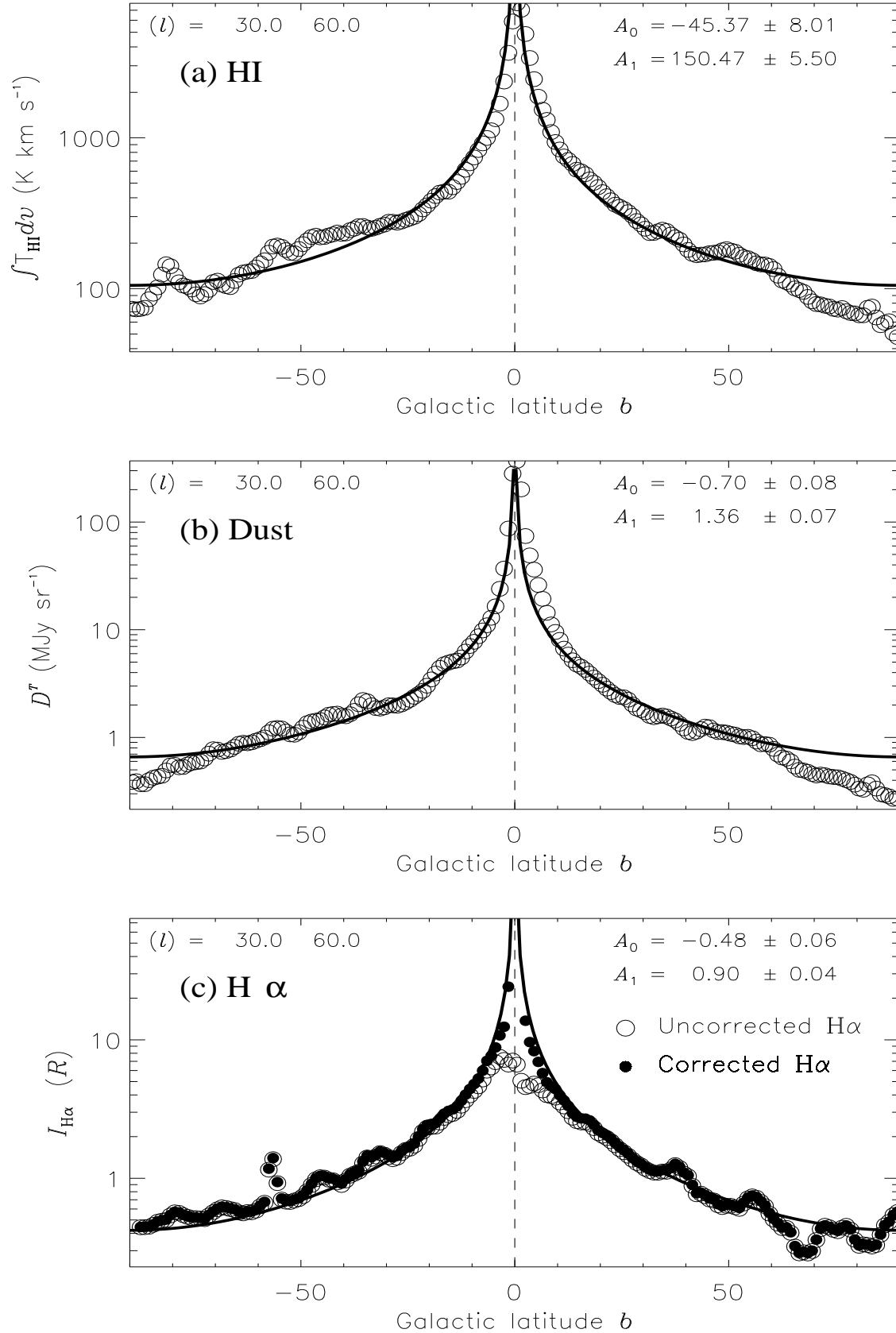


Figure 1. Galactic latitude scans for the longitude range $l = 30^\circ - 60^\circ$. (a) HI from Leiden-Dwingeloo survey data. (b) Dust emissivity at $100 \mu\text{m}$ from the SFD98 D^T template. (c) H α data from the WHAM survey. In (c) the H α data corrected for dust absorption ($f_d = 0.33$) are shown as filled circles while the uncorrected data are open circles. The best-fitting cosecant law is shown for each distribution (see text). Note the logarithmic scale on the vertical axes.

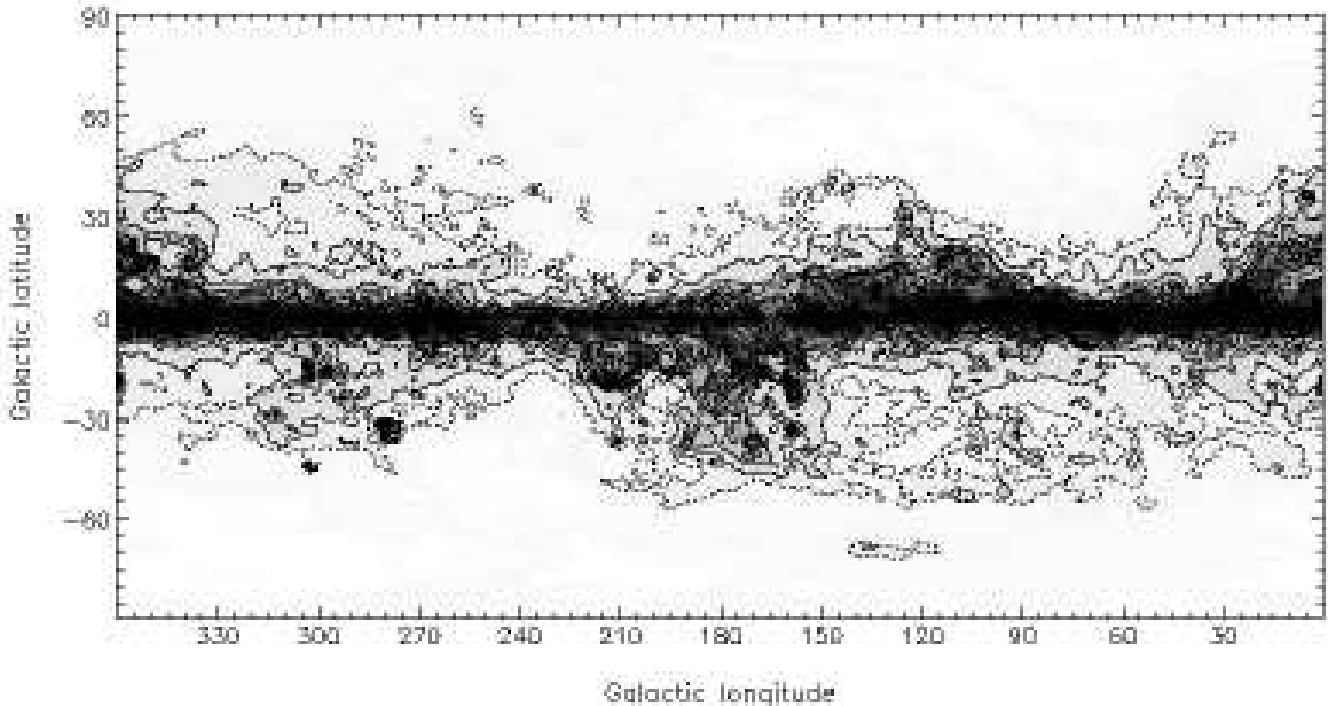


Figure 2. The absorption template to be applied to the Galactic $H\alpha$ emission. This assumes an absorbing dust-fraction of $f_d = 0.33$, as derived in Section 2.4, and the total extragalactic value $A(H\alpha)$ given in equation (1). Linear grey-scale and contours show absorption in magnitudes. Contours are given at 0.05 (dot-dashed), 0.1, 0.2, 0.3, 0.4, 0.5 and 0.7 mag. Absorption above 1 mag is black on the grey-scale.

It is interesting to note that the absorption can be low (< 0.5 mag) close to the Galactic plane in the longitude range $160^\circ < l < 260^\circ$. These regions may be useful in testing the dust absorption and $H\alpha$ templates at low latitudes. However, for the remainder of the Galactic plane ($|b| < 5^\circ$) the absorption is too great to make any reasonable estimate of $H\alpha$ emission.

The uncertainty in deriving the $H\alpha$ absorption from the dust using equation (1) is considered to be 20 per cent (see Section 2.2). A second factor in the uncertainty is the relative distribution of gas ($H\alpha$) and dust in the line of sight (f_d). Near the Galactic plane where there are many clouds/features in the line of sight, our value of $f_d = 0.33$ is realistic, while at higher latitudes where there are only a few clouds in the line of sight, the uncertainty (in a smaller total absorption) is greater. If we adopt a 20 per cent uncertainty in f_d and combine it with a 20 per cent error in equation (1), we obtain a total uncertainty of 30 per cent in the correction to the $H\alpha$ intensity for dust absorption. Thus if there is an $H\alpha$ absorption ($f_d \times A(H\alpha)$) of 1.0 mag, the 30 per cent uncertainty in multiplying factor required to give the estimate of the true $H\alpha$ intensity is 2.5 ± 0.7 . However for a total absorption of 0.2 mag the multiplying factor is 1.20 ± 0.07 . This illustrates the higher fractional accuracy of estimating the $H\alpha$ intensity at lower levels of absorption. In summary, the absorption of $H\alpha$ can be estimated up to a limit of ~ 1 mag; this corresponds to $D^T = 65 \text{ MJy sr}^{-1}$ for $f_d = 0.33$ and is shown as black on Fig. 2.

3 CONVERSION OF $H\alpha$ TO FREE-FREE CONTINUUM EMISSION

The ionized interstellar medium generates both radio free-free continuum and $H\alpha$ emission. Ionized hydrogen alone is responsible for the $H\alpha$ emission while ionized hydrogen and helium produce the radio continuum. Both the optical and radio emission are functions of electron temperature, T_e . A relationship between the two can be determined on certain assumptions. We will derive this relationship and give an estimate of the uncertainties which come from the theory and from the variation in the electron temperature at different locations within the Galaxy.

3.1 $H\alpha$ emission

The Balmer line emission from ionized interstellar gas is well understood; a clear discussion is given by Osterbrock (1989). However, the $H\alpha$ line intensity depends upon whether the emitting medium is optically thick (case B) or optically thin (case A) to the ionizing Lyman continuum. In the HII regions and nebulae studied using $H\alpha$ it is believed that case B applies (Osterbrock 1989). Knowing the emission coefficients for both case A and case B for $H\beta$ and using the Balmer decrements (Hummer & Storey 1987), the $H\alpha$ emission can be readily calculated for the temperature range 5000 – 20000 K both for case A and case B. Fig. 3 shows the $H\alpha$ intensity per unit Emission Measure ($EM \equiv \int n_e^2 dl$) for $T_e = 5000, 10000, 20000$ K for both case A and case B.

The emission coefficients are generally accepted to be accurate to ≈ 1 per cent (Pengelly 1964; Hummer & Storey

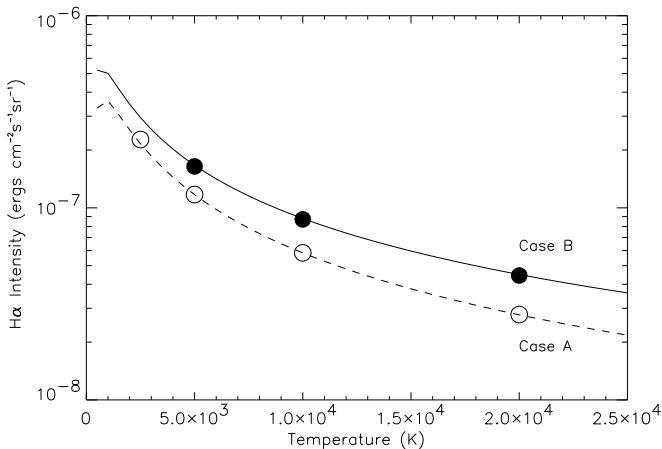


Figure 3. $H\alpha$ emission per unit Emission Measure as a function of T_e for case A (optically thin to Lyman photons) and case B (optically thick to Lyman photons) for $n_e = 10^2 \text{ cm}^{-3}$. The circles represent the values calculated by theory given by Hummer & Storey (1987). The curves are the expressions given by Valls-Gabaud (1998); case B is given in equation (4).

1987). For case B, the intensity varies very weakly with number density, amounting to a few percent over 2 orders of magnitude in density. The values shown in Fig. 3 are for a density ($n_e = 10^2 \text{ cm}^{-3}$) gas. Case A gives ≈ 30 per cent lower intensity than case B over the likely temperature range.

The situation for intermediate and high latitudes appears to favour case B on the following arguments. For case B to apply, the optical depth τ , to Lyman continuum photons ($\lambda \lesssim 900 \text{ \AA}$) must be greater than unity in the emitting region. Pottasch (1983) gives the mean free path of Lyman continuum photons as $\approx 0.052 n_H^{-1} \text{ pc}$, corresponding to an optical depth relation $\tau = 19.2 n_H l$ where l is path length in pc. For a typical HII region in the Galactic plane $n_e \approx n_H = 10^2 - 10^6 \text{ cm}^{-3}$ on typical scales of 1 – 10 pc and case B conditions are clearly satisfied with $\tau \approx 10^3 - 10^{10}$. At intermediate latitudes faint $H\alpha$ features with $EM \sim 1 \text{ cm}^{-6} \text{ pc}$ can be identified with scale sizes of $\sim 10 - 100 \text{ pc}$. The corresponding n_e is 0.1 – 0.3 cm^{-3} . The optical depth to Lyman continuum in these low density regions is then 1 – 30, still satisfying the case B conditions.

A useful and accurate expression for the $H\alpha$ intensity based on data from Hummer & Storey (1987) is given by Valls-Gabaud (1998) for case B in units of $\text{erg cm}^{-2} \text{ s}^{-1} \text{ sr}^{-1}$:

$$I(H\alpha) \stackrel{\text{Case B}}{=} 9.41 \times 10^{-8} T_4^{-1.017} 10^{-0.029/T_4} \times (EM)_{\text{cm}^{-6} \text{ pc}} \quad (4)$$

where T_4 is the electron temperature in units of 10^4 K . This is plotted as a continuous curve along with the equivalent curve for case A in Fig. 3, which shows that the agreement of equation (4) with theory is better than 1 per cent over the temperature range 5000 – 20000 K.

3.2 Radio continuum emission

The free-free radio continuum emission for an ionized gas at $T_e < 550,000 \text{ K}$ and in Local Thermal Equilibrium (LTE) is well described in terms of a volume emissivity in units of $\text{erg cm}^{-3} \text{ s}^{-1} \text{ Hz}^{-1}$ (Oster 1961):

Table 2. Gaunt factors for relevant frequencies and electron temperatures calculated from Hummer (1988) and accurate to 0.7 per cent.

ν (GHz)	T_e (K)				
	4000	6000	7000	8000	10000
0.4	5.82	6.03	6.11	6.18	6.39
1.4	5.16	5.37	5.45	5.52	5.73
2.3	4.90	5.11	5.19	5.26	5.47
10	4.13	4.34	4.42	4.49	4.70
30	3.55	3.76	3.84	3.91	4.12
44	3.35	3.56	3.64	3.71	3.92
70	3.10	3.32	3.40	3.45	3.67
100	2.92	3.13	3.21	3.28	3.49

$$\epsilon_{\nu}^{ff} = 6.82 \times 10^{-38} Z^2 n_e n_{\text{ion}} T_e^{-1/2} e^{-h\nu/kT} \langle \bar{g}_{ff}^{-1} \rangle \quad (5)$$

Here $\langle \bar{g}_{ff}(Z, \nu, T_e) \rangle$ is the velocity-averaged Gaunt factor. The Gaunt factor comprises all the terms by which the quantum mechanical expressions differ from the classical ones. The evaluation of the Gaunt factor has been refined over recent years since the work of Scheuer (1960) and Oster (1961) for a range of frequencies, temperatures. Karzas & Latter (1961) have given definitive expressions for \bar{g}_{ff} . Hummer (1988) has used these expressions to obtain an accurate analytical expansion for \bar{g}_{ff} in terms of a two-dimensional Chebyshev fit covering a wide range of frequencies and temperatures. Table 2 lists accurate Gaunt factors (accurate to 0.7 per cent) derived from Hummer (1988) for a range of frequencies and temperatures relevant to CMB studies.

We now summarize the present situation for the frequencies (0.4 – 100 GHz) covered by the observations analysed here and the observing range of the Low Frequency Instrument (LFI) on the *Planck* Surveyor satellite. The free-free spectral index β_{ff} is a slow function of frequency and electron temperature (Bennett et al. 1992) as shown in Fig. 4. Over a wide range in frequencies this can lead to a significant discrepancy in the predicted radio emission if this is not accounted for. One should therefore still use the accurate formalism given by Oster (1961) who derives the optical depth for free-free emission as

$$\tau_c(\text{Oster}) = 3.014 \times 10^{-2} T_e^{-1.5} \nu_{\text{GHz}}^{-2.0} \times \{ \ln[4.955 \times 10^{-2} \nu^{-1}] + 1.5 \ln(T_e) \} \times (EM)_{\text{cm}^{-6} \text{ pc}} \quad (6)$$

The approximation given by Altenhoff et al. (1960) is often used:

$$\tau_c(\text{AMWW}) = 8.235 \times 10^{-2} T_e^{-1.35} \nu_{\text{GHz}}^{-2.1} \times (EM)_{\text{cm}^{-6} \text{ pc}} \quad (7)$$

For low frequencies ($\lesssim 1 \text{ GHz}$) the error in this expression is of the order a few percent but increases to 5-20 per cent for frequencies above 10 GHz. Mezger & Henderson (1967) define a factor $a(T, \nu)$, the ratio between the two formulae as

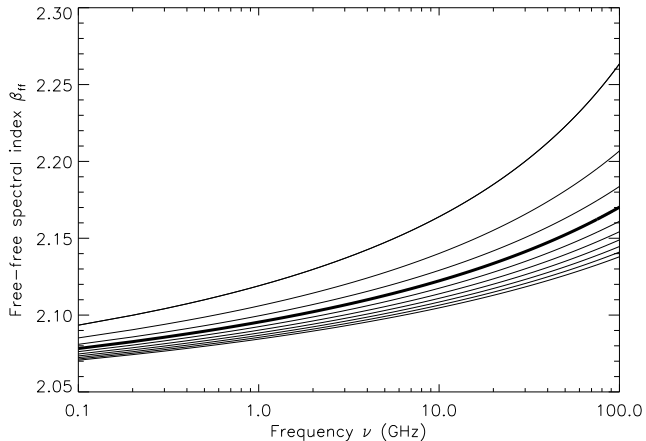


Figure 4. The local free-free spectral index as a function of frequency and electron temperature; given by equation (3) of Bennett et al. (1992). The curves from top to bottom are for temperatures $T_e = (2, 4, 6, 8, 10, 12, 14, 16, 18, 20) \times 10^3$ K.

Table 3. The factor $a = \tau_c(\text{Oster})/\tau_c(\text{AMWW})$ for relevant frequencies and temperatures using equation (8).

ν (GHz)	T_e (K)				
	4000	6000	7000	8000	10000
0.4	0.9972	0.9934	0.9912	0.9889	0.9844
1.4	0.9936	0.9974	0.9978	0.9977	0.9967
2.3	0.9872	0.9946	0.9962	0.9972	0.9978
10	0.9484	0.9684	0.9745	0.9792	0.9857
30	0.8957	0.9276	0.9379	0.9461	0.9582
44	0.8717	0.9084	0.9203	0.9299	0.9442
70	0.8382	0.8810	0.8952	0.9066	0.9238
100	0.8090	0.8569	0.8729	0.8858	0.9054

$$a = \frac{\tau_c(\text{Oster})}{\tau_c(\text{AMWW})} = 0.366 \nu_{\text{GHz}}^{0.1} T_e^{-0.15} \times \left\{ \ln[4.995 \times 10^{-2} \nu_{\text{GHz}}^{-1}] + 1.5 \ln(T_e) \right\} \quad (8)$$

Table 3 gives accurate values of a based on equation (8) for a range of temperatures and frequencies. The a factor is convenient in that it allows a simple formula to be written down using a single spectral index and temperature dependence which are modified by the Gaunt factor.

The brightness temperature T_b is given by

$$T_b = T_e(1 - e^{-\tau_c}) \approx T_e \tau_c \quad \text{for } \tau_c \ll 1 \quad (9)$$

For the frequencies relevant to CMB observations and the diffuse interstellar medium discussed here, the optically thin assumption is valid. At 1 GHz only the brightest HII regions in the Galaxy are optically thick ($EM \geq 10^6 \text{ cm}^{-6} \text{ pc}$) while the Galactic ridge has $\tau \sim 10^{-3}$ ($EM \geq 10^3 \text{ cm}^{-6} \text{ pc} \approx 500 R$) estimated for $T_e = 7000$ K.

Finally, the brightness temperature in Kelvin can now be written as

$$T_b = 8.235 \times 10^{-2} a T_e^{-0.35} \nu_{\text{GHz}}^{-2.1} (1 + 0.08) \times (EM)_{\text{cm}^{-6} \text{ pc}} \quad (10)$$

where the factor $(1+0.08)$ is the contribution from the fraction of He atoms, all of which are assumed to be singly ionized; a is given by equation (8).

3.3 Electron temperatures in Galactic HII regions

Optical determinations of electron temperatures in HII regions using forbidden line ratios give values in the range 5000 to 20000 K with a mean value of ≈ 8000 K (Reynolds 1985). These determinations refer to the solar neighbourhood within 1 or 2 kpc of the Sun.

Electron temperature determinations using extensive radio recombination line (RRL) data probe the greater part of the Galaxy and show a clear temperature gradient as a function of galacto-centric radius. The results of Shaver et al. (1983) for 67 HII regions show a clear gradient in temperature increasing with galacto-centric radius from 5000 K at 4 kpc to 9,000 K at 12 kpc. This is due to the decreasing metallicity at larger radii (Panagia 1979). There is a spread of approximately 1000 K at a particular radius. The local value at $R_0 = 8.5$ kpc is $T_e = 7000$ K and will be adopted as the typical value in the absence of other information.

3.4 Expected radio emission from H α maps

The relationship between radio emission and H α emission can now be calculated using equations (4) and (10), in units of mK/R as

$$\frac{T_b^{ff}}{I_{H\alpha}} = 8.396 \times 10^3 a \times \nu_{\text{GHz}}^{-2.1} T_4^{0.667} 10^{0.029/T_4} (1 + 0.08) \quad (11)$$

where T_4 is the electron temperature in units of 10^4 K. The conversion factors for relevant frequencies are given in Table 4 for $T_e = 7000$ K. Fig. 5 shows $(T_b^{ff}/I_{H\alpha}) \nu_{\text{GHz}}^2$ over the frequency range 100 MHz to 100 GHz for $T_e = 4000, 7000, 10000$ and 15000 K. The increase in (negative) slope with frequency is due to the effect of a arising from the Gaunt factor dependence. The variation in T_b^{ff} at a given frequency corresponds to a factor of ~ 2.4 between 4000 and 15000 K.

It is of interest to compare our equation (11) with recent expressions given in the literature. Reynolds & Haffner (2002) give $T_b^{ff}/I_{H\alpha} = 7.4 \nu_{30}^{-2.14} \mu\text{K}/R$ at $T_e = 8000$ K. Our value at 30 GHz and 8000 K would be 17 per cent lower at 6.35 $\mu\text{K}/R$. This difference may be attributed to the 17 per cent over-estimate of the Gaunt factor in equation (6) of Valls-Gabaud (1998) which are used by Reynolds & Haffner (2002). We have resolved this difference with help from David Valls-Gabaud (private communication). The coefficient in his equation (6) should be 3.96 and not 4.4; furthermore, a typographical error in his equation (11) gave the exponent of T_4 as 0.317 instead of 0.517. He agrees with the calculations of the Gaunt factors in Section 3.2. His new calculations also agree well with our equation (11). Equation (4), also from Valls-Gabaud (1998), is not affected.

The uncertainty in predicting the radio free-free emission from the H α emission as given in equation (11) arises

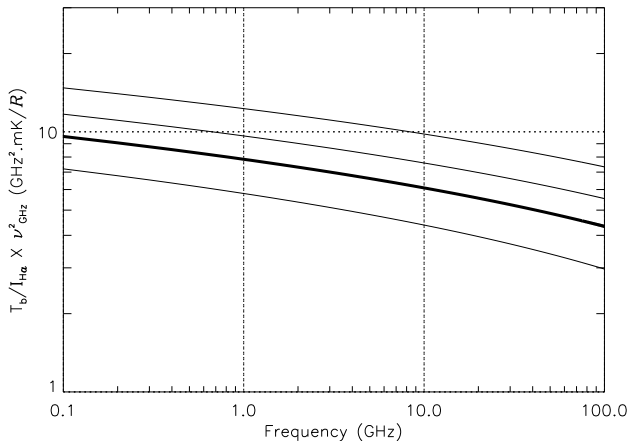


Figure 5. Ratio of radio brightness temperature to $H\alpha$ intensity multiplied by ν_{GHz}^2 as a function of frequency. Curves are for $T = 4000, 7000$ [heavy], 10000 and 15000 K which is the likely temperature range corresponding to a factor ~ 2.4 in the ratio. The curvature in each curve reflects the frequency dependence of the Gaunt factor.

Table 4. Free-free brightness temperatures per unit Rayleigh for a range of frequencies assuming $T_e = 7000$ K.

Frequency [GHz]	Free-free brightness temperature per unit Rayleigh
0.408	51.2 mK
1.420	3.76 mK
2.326	1.33 mK
10	60.9 μ K
30	5.83 μ K
44	2.56 μ K
70	0.94 μ K
100	0.43 μ K

mainly from the uncertainty in the electron temperature. The ± 1000 K uncertainty in the adopted solar neighbourhood value of 7000 K is an upper limit to the scatter of HII region temperatures since it includes some measurement errors. The corresponding error in equation (11) is 10 per cent. The other possible uncertainty is in whether case A or case B applies in the lower density regions at intermediate and high Galactic latitudes of interest to CMB studies. For the reasons given in Section 3.1, we will adopt the generally assumed position that case B is correct and take the associated error in equation (4) to be 1 per cent. However, in the unlikely event that case A were to apply, the value of $T_b/I_{H\alpha}$ given in equation (11) would be increased by 30 per cent. Uncertainties in equation (4) and in the ionized helium to hydrogen ratio in equation (10) are only a few per cent. We consider that the overall uncertainty in applying equation (11) to be ~ 10 per cent for a large sample of the sky, assuming case B applies.

4 OBSERVATIONAL TESTS OF THE $H\alpha$ TO FREE-FREE RELATION

We now make an observational test of equation (11) which predicts the free-free radio emission for a given $H\alpha$ intensity. In practice, the diffuse free-free emission is mixed with synchrotron emission so the free-free component must be identified and separated. The free-free emission can be identified in two ways. Firstly, by its associated radio recombination line emission and secondly, by its free-free spectrum using multi-frequency observations. Furthermore, a comparison between the radio and $H\alpha$ will lead to an estimate of the $H\alpha$ absorption by dust; this can be compared with $A(H\alpha)$ given by equation (1) to give a value of the absorbing factor of dust f_d in front of the $H\alpha$.

4.1 Radio Recombination Lines

One advantage of using radio recombination lines (RRL's) is that the ratio of the line temperature to continuum temperature can be used to derive an electron temperature T_e for the HII emission which can be substituted in equation (11) to give the radio emission expected from the observed $H\alpha$ emission. Two extended regions of $H\alpha$ emission which are sufficiently bright to have been studied in RRL's are Barnard's Arc and the Gum Nebula.

4.1.1 Barnard's Arc

Barnard's Arc is an ionization-bounded HII region at 460 pc photo-ionized by the Orion I OB star association (Reynolds & Ogden 1979). At radio frequencies Barnard's Arc has a thermal spectral index (Davies 1963). Gaylard (1984) describes RRL observations at 2.272 GHz at 3 positions in the Arc. The radio data were converted from antenna to brightness temperatures using the factor 1.5 used by Gaylard (1984). The $H\alpha$ observations from SHASSA and the D^T dust map were smoothed to 20 arcmin resolution for this study. Table 5 gives the observed brightness temperature T_b , T_e and $T_{H\alpha}$, the brightness temperature expected from the observed $H\alpha$ intensity $I_{H\alpha}$, uncorrected for absorption using T_e values also given in Table 5. The small (< 10 per cent) errors in the radio data for the 3 positions in Barnard's arc, indicate that the calculated f_d values are accurate to about ± 0.15 and are therefore consistent with no or little absorption ($f_d \sim 0$) in all 3 positions. No absorption would be expected if the $H\alpha$ -emitting gas were nearer than the dust, in this nearby (< 500 pc) Gould Belt feature.

4.1.2 The Gum Nebula

The Gum Nebula is a diffuse emission region centred on $(l, b) = (258^\circ, -2^\circ)$ (Gum 1952). It is a complex at a distance of 500 pc containing both free-free and synchrotron features which are probably the consequence of supernova activity (Duncan et al. 1996; Reynosa & Dubner 1997). The RRL data from Woermann et al. (2000) for $H\alpha$ features within the complex taken with 20 arcmin resolution are compared with the $H\alpha$ and dust data as in Section 4.1.1 and are given in Table 5. The data tabulated are for the 3 strongest

Table 5. Comparison of the observed brightness temperature T_b from RRL data with the predicted brightness temperature $T_{H\alpha}$ from $H\alpha$ data using equation (11). The first three positions are in Barnard’s Arc (Gaylard 1984) and the next three are in the Gum Nebula (Woermann et al. 2000). Using the dust column density D^T and electron temperature T_e , the fraction of f_d dust causing absorption of $H\alpha$ emission is calculated for each observation.

Coordinates (B1950/Galactic)	Frequency [MHz]	T_b [mK]	T_e [K]	$I_{H\alpha}$ [R]	$D_{100\mu m}^T$ [MJy sr $^{-1}$]	$T_{H\alpha}$ [mK]	f_d
$5^h 49^m + 00^\circ 38^m$	2272.661	295 ± 24	5200 ± 400	280 ± 24	21.2	330	-0.1
$5^h 51^m - 01^\circ 00^m$	2272.661	280 ± 18	3800 ± 300	170 ± 15	15.2	269	+0.1
$5^h 54^m - 02^\circ 45^m$	2272.661	258 ± 14	6600 ± 1100	188 ± 17	17.2	254	0
G264.00 -12.80	1715.67	450 ± 105	8500 ± 2400	223 ± 20	6.7	673	-1.4
	2422.46	263 ± 53	7800 ± 2300	223 ± 20	6.7	310	-0.6
G265.00 -08.00	1715.67	570 ± 120	5700 ± 1400	232 ± 21	12.0	535	+0.1
G270.65 +10.40	1715.67	398 ± 90	5800 ± 1400	123 ± 11	6.2	302	+1.0

$H\alpha$ features in the Gum Nebula. There is a large spread in f_d values from -1.4 to $+1.0$. The large error bars on the radio data (T_b, T_e) correspond to an error of approximately ± 0.6 to ± 1.0 in the derived f_d values for the three Gum nebula positions. Little can be deduced about the value of f_d without better radio data; negative values have no physical meaning except that the $H\alpha$ prediction is larger than is measured in the radio.

4.2 Multi-frequency scans across $H\alpha$ features

An alternative method of identifying and measuring the radio free-free emission from an $H\alpha$ feature is to use multi-frequency scans across it to separate the free-free from the underlying synchrotron emission. The brightest features of Barnard’s Arc are ideal since they lie some 20° from the Galactic plane where the background synchrotron emission is weak and relatively smooth. We have used the 408 MHz map of Haslam et al. (1982) in the destriped form given by Davies et al. (1996) and the 2326 MHz map of Jonas et al. (1998) to make 3 Galactic longitude scans across the Barnard Arc feature at $b = -18^\circ, -20^\circ$ and -22° centred on $l \sim 212^\circ$. These are illustrated in Fig. 6 along with the corresponding $H\alpha$ scans from WHAM data; all data are at a resolution of 1° . The amplitudes of the best-fitting gaussians to the feature centred on each $H\alpha$ position are given in Table 6. Values of f_d are estimated as in Section 4.1 for $T_e = 7000$ K (the average local value) and $T_e = 5100$ K (the weighted average of T_e from Table 5). The derived f_d values are accurate to about ± 0.1 to ± 0.2 and are significantly negative when $T_e = 7000$ K is assumed, indicating the radio emission is greater than expected from the $H\alpha$ brightness with no foreground absorption. However, when the average measured value of T_e (5100 K) is used, the derived f_d values are consistent with no absorption ($f_d = 0$). This clearly shows the importance of having accurate electron temperatures. In this case, the lower electron temperature corresponds to a ~ 25 per cent reduction in $T_{H\alpha}$. A further consideration is the full-beam to main-beam correction (see Sections 6 & 7) which can lead to a factor of ~ 1.5 for objects comparable in size to the beam. For Barnard’s Arc, which is extended

($\sim 5^\circ$) in one direction and ~ 1.5 in the perpendicular direction, the correction is likely to be the square root of this factor (~ 1.2). This further correction would lead to a slightly positive (~ 0.2) value for f_d .

4.3 Identifying $H\alpha$ morphology in radio maps

The morphology of extended bright $H\alpha$ regions can be identified in the low frequency continuum maps even in the presence of significant synchrotron emission. By subtracting a template from the radio continuum maps proportional to the $H\alpha$ intensity, it is possible to estimate the amplitude of the free-free emission. A first-order approach is illustrated for the Orion region in Fig. 7. The 408 MHz, 2326 MHz, WHAM $H\alpha$ and the D^T dust maps are first smoothed to 1° resolution. Different amplitudes of the free-free emission expected from the $H\alpha$ maps are subtracted from the radio maps until the correlation with the $H\alpha$ maps disappears from the radio maps; we are left with the synchrotron features only. Then using the absorption expected from the D^T dust map, an estimate is made of f_d for the field. In this case, assuming a nominal electron temperature of $T_e = 7000$ K, both the λ -Orionis nebula ($l, b \approx (195^\circ, -11^\circ)$) and Barnard’s Arc give $f_d = -0.2 \pm 0.1$, suggesting no dust absorption. The error bars are estimated by comparing maps with different amounts of $H\alpha$. As shown in Section 4.2, the effect of a lower average temperature for these regions and/or the full-beam to main-beam correction, may bring the $H\alpha$ estimate in agreement with the radio data ($f_d \geq 0$).

A similar study was made of the Gum Nebula where f_d was found to be -0.2 ± 0.2 , and the Ophiuchus HII region $l \approx (0^\circ) - (20^\circ), b \approx (+15^\circ) - (+30^\circ)$ where $f_d = 0 \pm 0.2$. The increased error in the estimate is due to the complexity of the emission across each region. In general, the $H\alpha$ predictions assuming $T_e = 7000$ K are correct when a factor of $0.7 - 1.0$ is included into the $H\alpha$ estimates (Fig. 7).

In summary, the raw $H\alpha$ predictions in these selected regions are slightly too large to fit the current low-frequency data by up to ~ 30 per cent. This may be accounted for by lower than average electron temperatures (probably the case

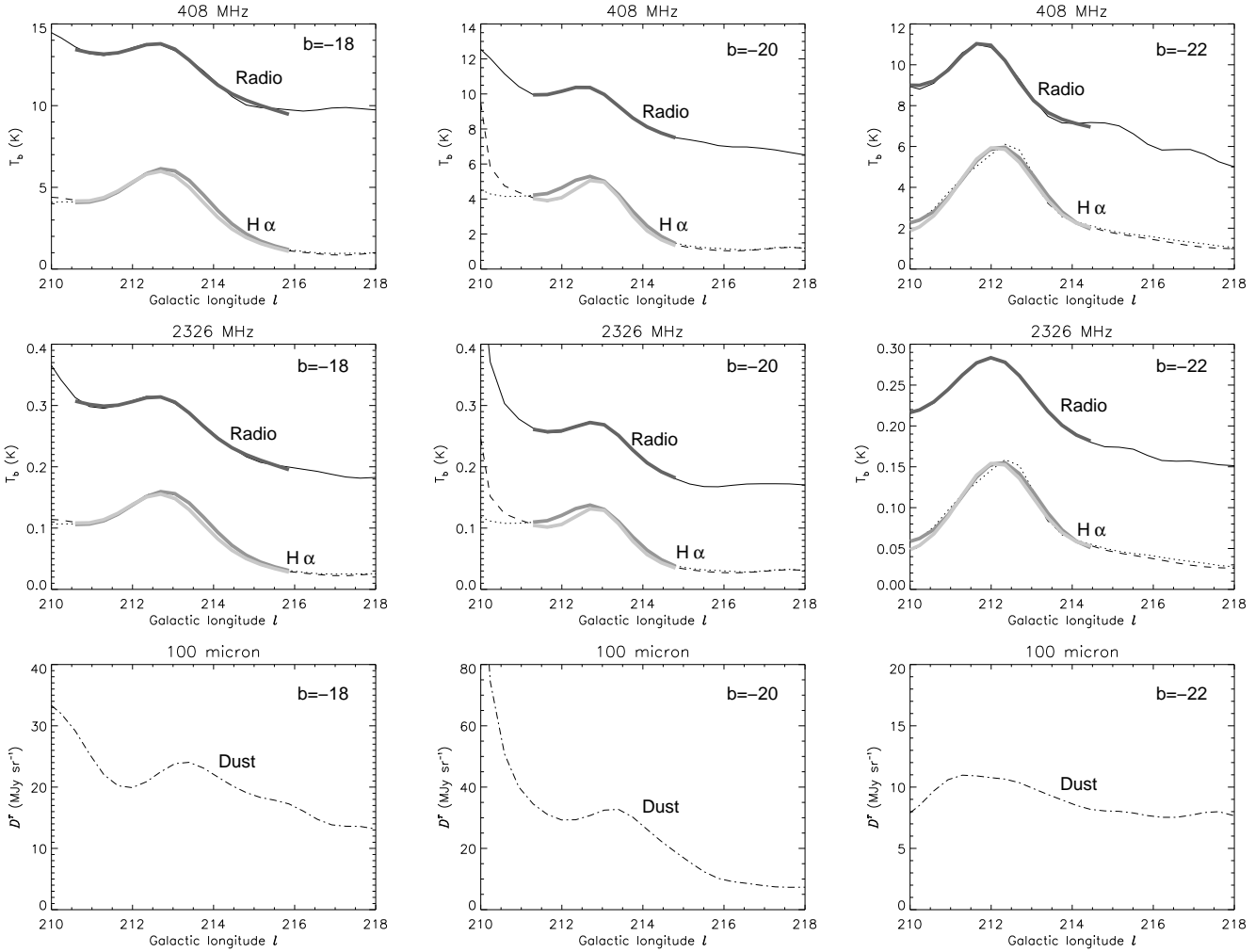


Figure 6. 408 and 2326 MHz scans across Barnard’s Arc at constant $b = -18^\circ$ (left), -20° (middle) and -22° (right). The top panels show the 408 MHz scan and the prediction from $H\alpha$; both WHAM and SHASSA are shown for each. WHAM is the dotted line and SHASSA is the dashed line. The best-fitting gaussian plus a linear baseline is shown as a heavy line; WHAM is the heavier line and SHASSA is the lighter line. The middle panels show 2326 MHz data and the same predictions as above for $H\alpha$. The bottom panel is the scan for D^T (SFD98).

Table 6. Comparison of the observed radio brightness temperature T_b with the prediction from $H\alpha$ data, $T_{H\alpha}$, for 3 scans across Barnard’s Arc at frequencies of 408 and 2326 MHz. The $H\alpha$ intensity $I_{H\alpha}$ and dust column density D^T are also listed. The expected brightness temperature $T_{H\alpha}$ and the associated dust fraction actually absorbing f_d are calculated for $T_e = 7000$ K (columns 7 & 8), and for $T_e = 5100$ K (columns 9 & 10) (see text).

Coordinates (l, b)	Frequency [MHz]	T_b [mK]	$I_{H\alpha}$ [R]	$D^T_{100\mu m}$ [MJy sr $^{-1}$]	$T_{H\alpha}$ [mK] ($T_e = 7000$ K)	f_d ($T_e = 7000$ K)	$T_{H\alpha}$ [mK] ($T_e = 5100$ K)	f_d ($T_e = 5100$ K)
(212.9°, -18°)	408	1980	67 ± 7	22.5	3400 ± 300	-0.6	2470 ± 220	-0.2
	2326	53	67 ± 7	22.5	89 ± 8	-0.5	64 ± 6	-0.2
(212.9°, -20°)	408	1490	47 ± 5	30.7	2400 ± 220	-0.4	1730 ± 160	-0.1
	2326	53	47 ± 5	30.7	62 ± 6	-0.1	45 ± 4	+0.1
(212.0°, -22°)	408	2990	80 ± 8	10.8	4100 ± 370	-0.7	2950 ± 270	0
	2326	89	80 ± 8	10.8	107 ± 10	-0.4	85 ± 8	+0.1

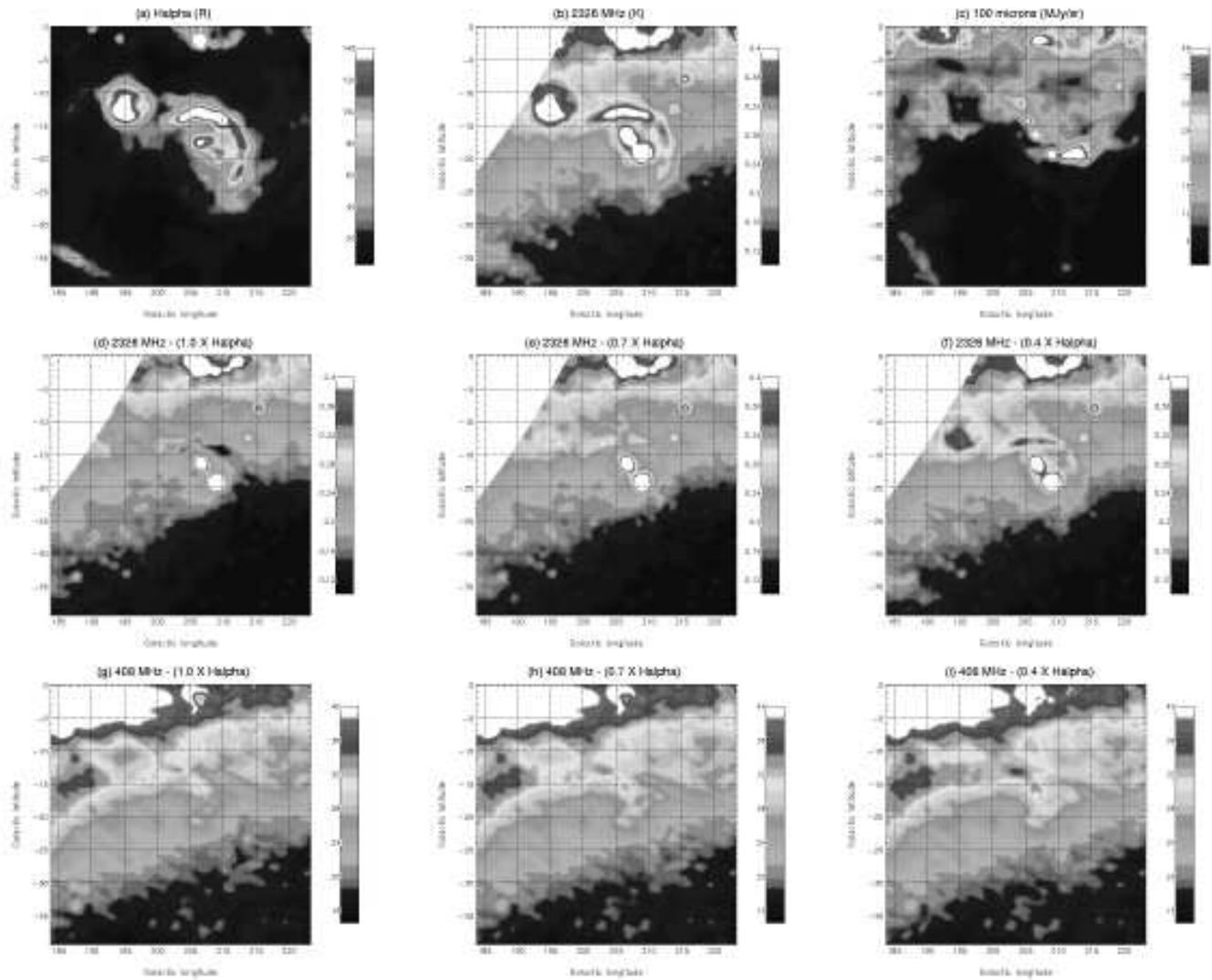


Figure 7. Morphology of the free-free component in the Orion region. (a) $H\alpha$ data from WHAM clearly shows Barnard’s Arc and λ -Orionis. (b) 2326 MHz data from Jonas et al. (1998) showing a similar morphology. (c) $100\ \mu\text{m}$ D^T map from SFD98 shows some correlation but not a one-to-one correlation. Panels (d,e,f) show the 2326 MHz map with varying levels (1.0, 0.7 and 0.4 multiplied by the conversions given in Table 4) of free-free emission subtracted as predicted by the $H\alpha$ data. Panels (g,h,i) are the same for the 408 MHz map from Haslam et al. (1982). The electron temperature is assumed to be $T_e = 7000$ K. The best subtraction occurs when the factor is ~ 0.7 . Note that no correction has been made for dust in this illustration and that the full-beam brightness temperature correction has not been applied (see text).

in some parts of the Orion region) which will vary the conversion factor from $H\alpha$ to radio continuum by up to ~ 30 per cent within a temperature range of 5000 – 10000 K. The full-beam to main-beam correction may also be a significant correction; up to 50 per cent, but ~ 20 – 30 per cent in elongated structures. The resulting f_d values for these regions are consistent with little or no absorption ($f_d \sim 0$). This might be expected since these regions are at relatively high Galactic latitudes ($|b| > 10^\circ$) and therefore nearby objects in which the geometry of the ionization, as seen from the Sun’s position in the Galactic plane, produces ionization on the near side of the gas/dust clouds.

5 THE BEST-ESTIMATE FREE-FREE TEMPLATE

We are now in a position to move from the observed $H\alpha$ maps of the northern and southern skies to produce a full-sky dust-corrected $H\alpha$ map at an angular resolution of 1° . Then, using equation (11) we can derive all-sky free-free maps except in areas near the Galactic plane where the predicted dust absorption becomes uncertain.

5.1 Full-sky $H\alpha$ map corrected for dust absorption

We obtain a full-sky $H\alpha$ map by using the northern WHAM $H\alpha$ data at 1° resolution and the higher angular resolu-

tion Southern SHASSA H α data. The H α map produced from WHAM data was made by interpolating the irregularly spaced data grid using the Interactive Data Language (IDL) routines TRIANGULATE and TRIGRID, which are based on Delauney triangulation, as suggested by the WHAM team (L.M. Haffner, private communication). The median filtered, continuum subtracted composite SHASSA map was used as given by the SHASSA team (J.E. Gaustad, private communication). Where the maps overlap, the WHAM map is used because of its higher sensitivity and better zero-level certainty, except for declinations $< -15^\circ$ where SHASSA data are preferred. The observed maps are regridded onto an over-sampled Cartesian Galactic coordinate grid and smoothed to 1° resolution. We then use the D^T map of $100 \mu\text{m}$ dust emission to correct for dust absorption at each point on the H α map according to equation (1). The fraction of the dust f_d lying in front of the H α is taken to be 0.33 as shown in Section 2.4 and discussed in Section 4.

Fig. 5.1 shows a colour representation of the dust-corrected full-sky H α map in Mollweide projection. Regions where the dust absorption correction is greater than 1.0 mag are shown as grey; H α data become unreliable in these regions. The Local System (Gould’s Belt) is clearly seen beneath the plane at $l \sim 180^\circ$ and above the plane at $l \sim 0^\circ$, reaching to $|b| \sim 30^\circ$ or more.

It should be remembered that both the WHAM and SHASSA surveys are in the early stages of analysis and further revisions are anticipated. Baseline effects are still visible in the data as presented in Fig. 5.1. For example, the WHAM data cannot accurately subtract the geocoronal emission near the ecliptic pole ($(l, b) \approx (96^\circ, 30^\circ)$), while the SHASSA data have artifacts due to the varying geocoronal emission in each $13^\circ \times 13^\circ$ field which results in a residual power on these scales in the region near $(l, b) \approx (320^\circ, -45^\circ)$. The typical level of these baseline variations are $\lesssim 1 R$.

5.2 A free-free all-sky template

We can now use Fig. 5.1 to produce an all-sky free-free template at any radio frequency using equation (11). For illustration we generate the template for 30 GHz, a frequency which is widely used for CMB studies such as the space projects *MAP* and *Planck* and the ground-based arrays CBI, DASI and VSA. In applying equation (11) we have taken $T_e = 7000$ K, the appropriate value for the region of Galaxy sampled by the H α maps at $|b| \gtrsim 10^\circ$. At 30 GHz, $T_b = 5.83 \mu\text{K}/R$ (Table 4).

The all-sky template for 30 GHz free-free emission is shown in Fig. 9. The amplitude of the free-free signal is $< 10 \mu\text{K}$ for $|b| > 30^\circ$ at most Galactic longitudes, although in the Local System T_b can be as large as $100 \mu\text{K}$. At higher frequencies the free-free emission falls as $\nu^{-2.15}$ and accordingly at 70 to 100 GHz, where foreground contamination of the CMB is least, the T_b values will be 5-10 times less than shown in Fig. 9. At these frequencies free-free and vibrational dust emission are the dominant foregrounds. Only the Galactic ridge ($|b| < 5^\circ - 10^\circ$) and isolated regions such as Orion have $T_b > 10 - 20 \mu\text{K}$ at frequencies 70 – 100 GHz.

We discuss the contribution of free-free emission to the CMB foregrounds in Section 7.3.

Table 7. Comparison of the r.m.s. fluctuations at 1° resolution of 408 MHz data and the free-free template for different Galactic latitude cuts. The all-sky value will be a lower limit since the corrections for dust are uncertain near the Galactic plane ($|b| < 5^\circ$).

Galactic cut	408 MHz r.m.s. (K)	Free-free r.m.s. (K)	Free-free / synchrotron ratio (%)
All-sky	30.3	2.9	> 10
$ b > 10^\circ$	10.3	0.85	8
$ b > 20^\circ$	7.2	0.39	5
$ b > 30^\circ$	5.9	0.23	4
$ b > 40^\circ$	5.1	0.08	2

6 AN IMPROVED LOW-FREQUENCY TEMPLATE

The 408 MHz all-sky map (Haslam et al. 1982) made at $0^\circ.85$ resolution is widely used as a template for the Galactic synchrotron foreground. Our present study allows us to correct this map for free-free emission at 408 MHz to obtain a clean synchrotron template. The free-free correction is estimated from the dust-corrected H α template of Fig. 5.1 using $T_b = 51.2 \text{ mK}/R$ as given by equation (11) and Table 4 with $T_e = 7000$ K.

Over much of the sky the free-free features are weaker than the synchrotron features at 408 MHz. However in regions such as the Local System at intermediate latitudes and the Gum Nebula at lower latitudes, the free-free features can be brighter than the synchrotron features. This is demonstrated in the Orion region in Fig. 7 where significant free-free emission is seen at both 408 MHz and 2326 MHz. In such regions the correction is clearly important.

To estimate the level at which free-free emission is present at 408 MHz, the r.m.s. fluctuation of the 408 MHz map smoothed to 1° resolution, are compared with that given by the free-free template map. Table 7 gives the results for different Galactic latitude cuts. The estimate of free-free contamination suggests that at high Galactic latitude ($|b| > 40^\circ$), away from bright H α features, the free-free component is a few per cent compared with the synchrotron component. At lower latitudes, the fraction increases to ~ 10 per cent. The all-sky value will be considerably underestimated since the corrections for dust absorption near the Galactic plane ($|b| < 5^\circ$) are uncertain. These estimates agree well with previous best estimates of the ratio of synchrotron and free-free. For example, the 10, 15 and 33 GHz Tenerife experiments combined with the 5 GHz Jodrell Bank interferometer show that the synchrotron and free-free components at intermediate latitudes are approximately equal at ~ 10 GHz (Jones et al. 2001). Assuming spectral indices of -3.0 and -2.1 for the synchrotron and free-free respectively, the ratio at 408 MHz extrapolated from 10 GHz predicts ~ 6 per cent of 408 MHz emission is in the form of free-free, in good agreement with the H α values given in Table 7.

Higher frequency maps will necessarily have higher fractions of free-free emission. The widely used maps at 1420 MHz (Reich & Reich 1988) and 2326 MHz (Jonas 1998) are used for estimating the Galactic contribution at higher fre-

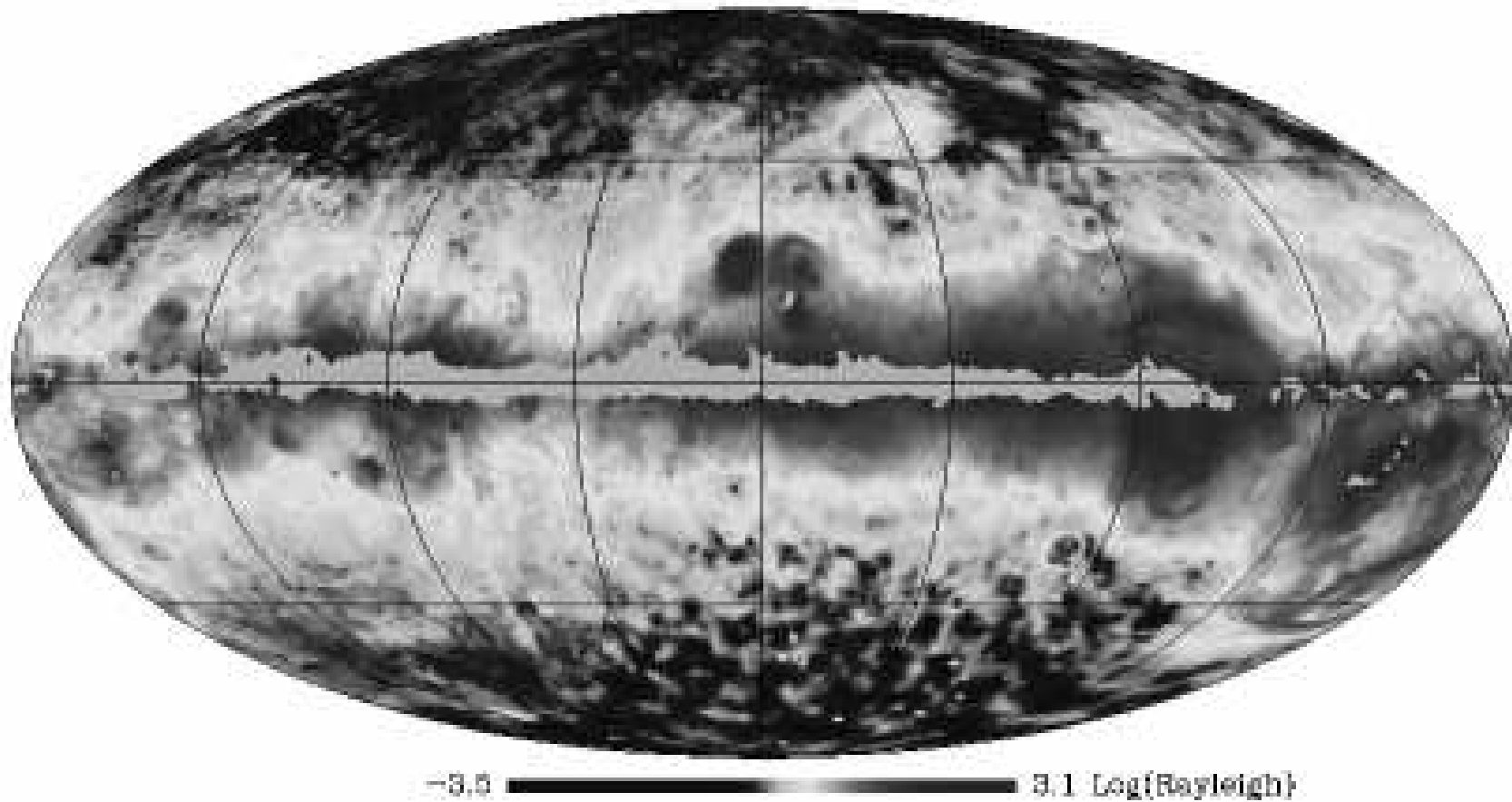
Full-sky dust corrected H α map

Figure 8. Full-sky dust-corrected H α map in Mollweide projection. The map has been repixelated into the HEALPix representation (Górski, Hivon & Wandelt 1999). The colour-scale has been histogram-equalized. Longitude $l = 0^\circ$ is in the centre and increasing to the left. Units are $\log(R)$. The composite map uses data from the WHAM survey (North) and the SHASSA survey (South) smoothed to a resolution of 1° . Data from WHAM is used in regions where data overlap for declinations $> -15^\circ$. The data are corrected for dust extinction up to a 1 mag of absorption assuming $f_d = 0.33$ derived in Section 2.4. Absorption above 1 mag is masked off as grey and depicts regions where the true H α absorption is uncertain. Baseline uncertainties are evident at high Galactic latitudes.

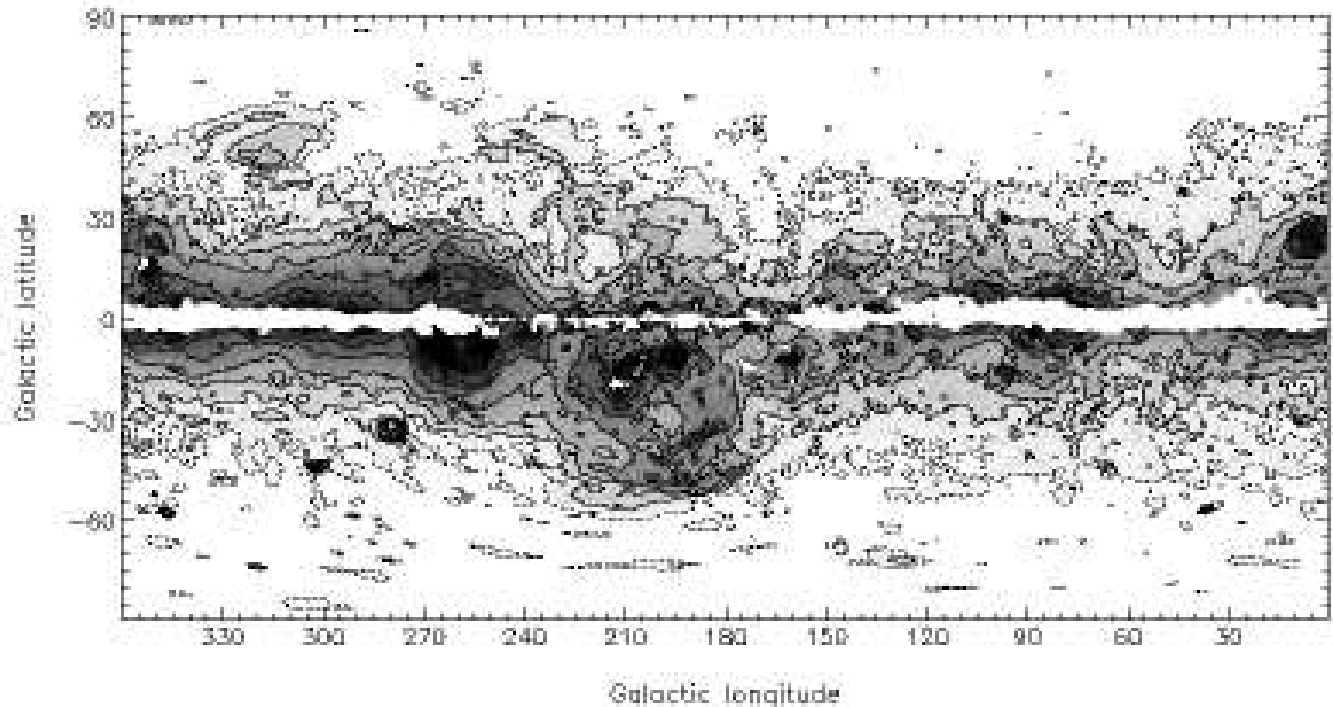


Figure 9. Free-free brightness temperature template at 30 GHz with 1° resolution. Grey-scale is logarithmic from 5 – 1000 μK . Regions where the template is unreliable are masked white. Contours are given at 5 (dot-dashed), 10,20,40,100,200 and 500 μK .

quencies. Using the estimate of 6 per cent at 408 MHz, the free-free fluctuations at 1420 MHz will contribute ≈ 15 per cent compared to the synchrotron component at intermediate latitudes, while at 2326 MHz this increases to ≈ 24 per cent. By correcting the 408 MHz map for free-free emission, a better synchrotron map can be made. This is particularly important for cross-correlation analyses which assume that the templates are not correlated.

With $\text{H}\alpha$ data alone it is not possible to construct a free-free correction template at lower Galactic latitudes. Fig. 5.1 shows regions along the Galactic plane where the dust absorption is too large to estimate an accurate dust-free $\text{H}\alpha$ intensity. We plan to use multi-frequency maps of the Galactic plane to separate the free-free and synchrotron components at low latitudes. The narrow free-free latitude distribution along the plane has a peak brightness at 408 MHz which varies from 40 to 80 per cent that of the broader synchrotron distribution at $l = 10^\circ$ to 50° (Large, Mathewson & Haslam 1961). Accordingly, the correction of the 408 MHz map for free-free emission is important at low latitudes.

The other factor in constructing a template at 1° resolution from the low frequency radio maps is the effect of the main-beam to full-beam ratio (~ 1.5) on angular scales of a few degrees; we note that the brightness temperature scale of the published maps is on the full-beam scale ($\sim 5^\circ - 10^\circ$). The result is that temperatures on the main-beam scale ($\sim 1^\circ$) should be multiplied by a factor ~ 1.5 to bring them to the correct brightness temperature scale. This procedure has been considered in Sections 4.2 and 4.3 and clearly needs to be taken into account for accurate free-free and synchrotron predictions. This scale-dependence to true brightness temperature has been noted before (e.g. Jonas et

al. 1998) and is currently under review when applying it to existing full-sky maps.

7 DISCUSSION

7.1 Precision of the free-free template

The $\text{H}\alpha$ intensities given by WHAM and SHASSA have quoted calibration accuracies of 10 and 9 per cent respectively. The corresponding zero level uncertainties are approximately 0.2 and 0.5 R . The accuracy is likely to be improved as these surveys are refined. The largest uncertainty in the $\text{H}\alpha$ intensity is in the dust absorption correction as discussed in Section 2. At intermediate and higher Galactic latitudes where $f_d \times A_{\text{H}\alpha} \leq 0.2$ mag, the error in the corrected $I_{\text{H}\alpha}$ is ≤ 5 per cent; this error increases to ~ 30 per cent where $f_d \times A_{\text{H}\alpha}$ is 1 mag nearer the Galactic plane.

On converting the dust-corrected $I_{\text{H}\alpha}$ to T_b , the free-free brightness temperature, a further uncertainty is introduced by the spread in T_e , the electron temperature, in the local region of the Galaxy covered by the $\text{H}\alpha$ maps. For $T_e = 7000 \pm 1000$ K, the T_b uncertainty is ± 10 per cent as derived from equation (11). As far as the emission theory used in Section 3 is concerned, we believe that the Gaunt factor and the analytical relations given are accurate to 1-2 per cent. It is assumed throughout that the $\text{H}\alpha$ emission is given by the case B emission formulae; the observed radio T_b values are consistent with this assumption.

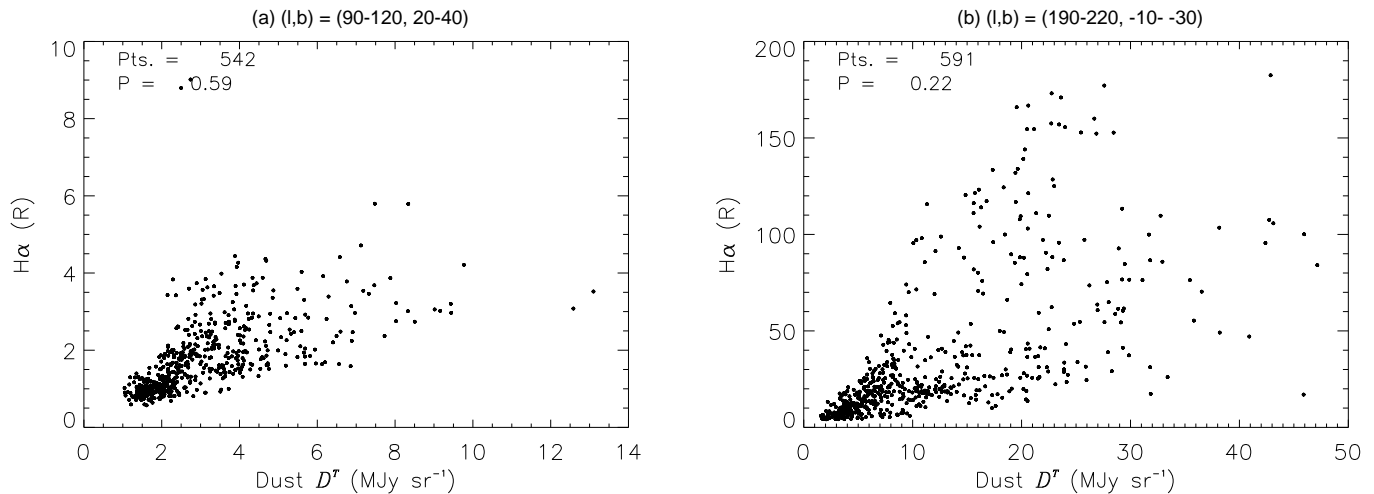


Figure 10. Correlation plots between H α and dust at a resolution of 1° for two regions (a) $l = (90^\circ - 120^\circ)$, $b = (20^\circ - 40^\circ)$ and (b) $l = (180^\circ - 210^\circ)$, $b = (-20^\circ \text{ to } -40^\circ)$. There is an overall positive correlation with considerable scatter. The Orion region (b) is brighter and shows a much larger scatter. The Pearson’s correlation coefficients are 0.59 and 0.22 respectively.

7.2 The contribution to other templates

A radio-independent method of determining a free-free template has a significant benefit in establishing the other Galactic foreground templates for CMB studies. We have already shown in Section 6 that an improved synchrotron template can be derived from the 408 MHz map by correcting for the known free-free emission. This method breaks down for the small area along the Galactic plane where the dust absorption of the H α becomes too high; other methods of determining the free-free emission are available here.

Spinning dust radiating in the region 10-40 GHz is proposed as a Galactic foreground (Draine & Lazarian 1998); observations appear to confirm this scenario (Kogut et al. 1996; Leitch et al. 1997; de Oliveira-Costa et al. 1997, 1998, 1999, 2000, 2002; Finkbeiner et al. 2002). A strong confirmation of the presence of spinning dust radio emission correlated with the SFD98 dust template requires a clean separation of the free-free component beforehand. This is important because the dust and H α are generally thought of as being correlated. An example of a region of the Galaxy where the correlation is relatively strong is $l = (90^\circ - 120^\circ)$, $b = (20^\circ - 40^\circ)$. This is illustrated in Fig. 10(a) which shows the correlation between H α and (D^T) from SFD98 at 1° resolution. The relation between $I_{\text{H}\alpha}$ and D^T for the region in Orion $l = (180^\circ - 210^\circ)$, $b = (-20^\circ \text{ to } -40^\circ)$ is given in Fig. 10 (b) where it is seen that the correlation is less strong. The distribution of H α and dust for the Orion region is shown in Fig. 11. The situation is clearly complex on the scale of 1° as would be expected for a star-forming region and underscores the necessity of removing the free-free emission before investigating spinning dust.

7.3 Free-free contribution to the CMB foregrounds

We will now estimate the free-free contribution to the CMB foregrounds at ~ 30 GHz. If not subtracted from the data, the foreground signal will add in quadrature to the CMB signal in the power spectrum since they will be uncorre-

lated on the sky. The free-free template allows statistical estimates to be made of the free-free component on angular scales $\gtrsim 1^\circ$ compared to the primordial CMB fluctuations. At angular scales of 1° ($\ell \approx 200$), the CMB has r.m.s. fluctuations of $\approx 75 \mu\text{K}$, falling to $\approx 30 \mu\text{K}$ at smaller and larger angular scales. Over a large portion of the higher latitude sky ($|b| > 40^\circ$), the average contribution of free-free emission is $\approx 9 \mu\text{K}$ at 30 GHz on scales of 1° . This amounts to a 1 per cent increase in the power spectrum at $\ell = 200$. However, individual regions may be contaminated at a much higher level depending on their position. At higher frequencies ($\sim 70 - 100$ GHz), the free-free contribution will be $\lesssim 1 \mu\text{K}$ and will be negligible at high latitudes.

We can also compare the estimates for specific regions of the sky where CMB observations have been made. The VSA has observed three regions of the sky measuring angular scales of $\approx 0.3 - 2.0$ ($\ell \approx 150 - 900$) covering a total area of 101 square degrees at a frequency of 34 GHz (Taylor et al. 2002). The contamination from free-free emission using the free-free template is estimated to give an r.m.s. temperature of $0.6 - 0.8 \mu\text{K}$ at the 1° scale and hence the free-free contamination is negligible in these selected regions.

The North Celestial Pole (NCP) region has been studied by the Saskatoon group (Wollack et al. 1997). The Saskatoon data show an anomalous component which cannot be explained on conventional grounds. Using the free-free template, the r.m.s. variations are $\approx 3.4 \mu\text{K}$ in a 15° -diameter circle centred on the NCP on smoothing the H α map to a resolution of 1.45 and assuming a conversion factor of $\approx 7 \mu\text{K}/R$. Simonetti et al. (1996) use their H α data to estimate an upper limit of $4.6 \mu\text{K}$ at 27.5 GHz in this region. These values of $\sim 4 \mu\text{K}$ can be compared with the $\approx 40 \mu\text{K}$ r.m.s. variations in the Saskatoon data. It therefore seems clear, that the anomalous emission is not in the form of free-free emission from gas at $T_e \sim 10000$ K. The current view is that it may be due to spinning dust emission as proposed by Draine & Lazarian (1998).

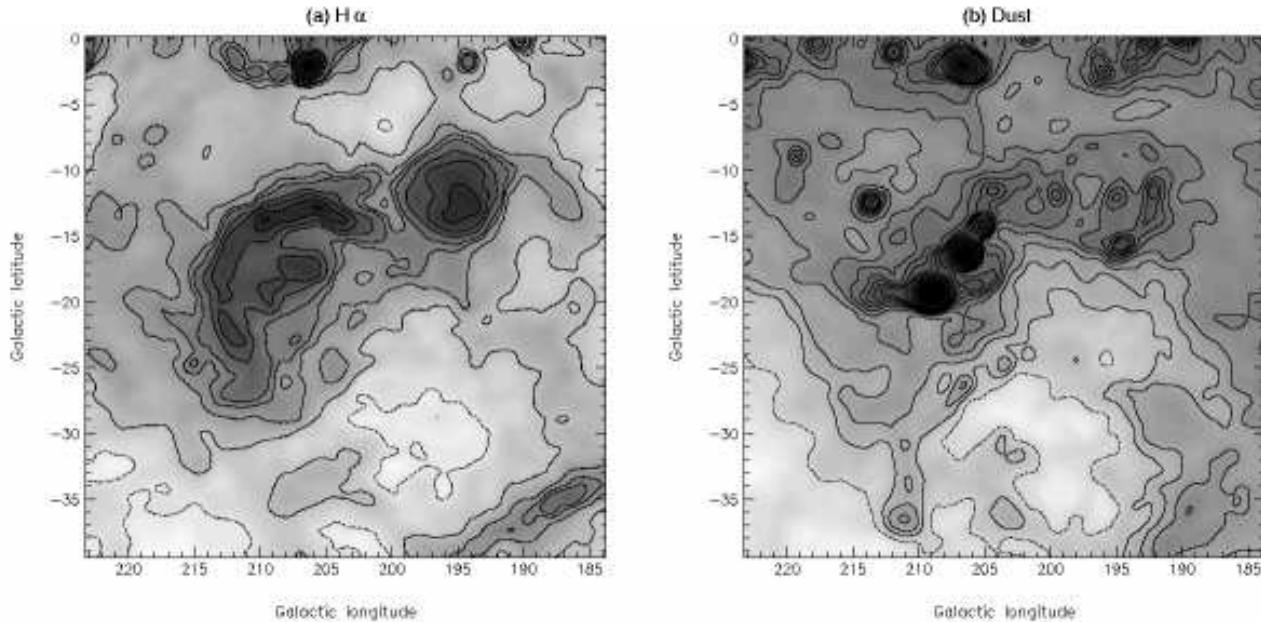


Figure 11. Correlations between H α and dust in the Orion region. (a) H α data from WHAM shown as a logarithmic grey-scale from 3 to 380 R and contoured at 5 (dot-dashed), 10, 20, 30, 40, 70, 100, 150 and 200 R . (b) 100 μm data from SFD98 depicting the dust in a logarithmic grey-scale from 0.1 to 200 MJy sr^{-1} and contoured at 3 (dot-dashed), 5, 7, 10, 15, 20, 25, 30, 35, 40, 50, 70 and 100 MJy sr^{-1} . There is an overall correlation between H α and dust but it is not one-to-one.

8 CONCLUSIONS

The recent publication of H α surveys covering the majority of the sky has provided a break-through in obtaining a free-free Galactic foreground template of importance for CMB and ISM studies. Having derived the free-free template it is then possible to determine a better synchrotron template and to make real progress in constructing a spinning dust template. The free-free template has many other applications which include a re-analysis of the *COBE-DMR* data (Banday et al., in preparation) and a free-free power spectrum analysis (Dickinson et al., in preparation).

We can look forward to an improved all-sky free-free template at higher resolution than the 1° used in the present work. A combination of the high resolution (arcmin scale) narrow-band filter surveys such as SHASSA and VTSS combined with the high sensitivity Fabry-Perot survey at a 1° scale would be ideal. At lower Galactic latitudes where the dust absorption of the H α emission is significant, multi-frequency continuum surveys should be able to separate the strong synchrotron and free-free components. Recombination line surveys such as those being undertaken with HIPASS in the South (Barnes et al. 2001) and HIJASS in the North (Kilborn 2002) will provide a confirmation of the low latitude free-free template and distinguish it from spinning dust which will have a very similar latitude distribution. The recombination line data will also lead to a kinematic 2-dimensional picture of the ionized gas distribution in the Galaxy using kinematic distances since they contain velocity information.

Acknowledgments

CD acknowledges a PPARC research grant. WHAM is funded by the National Science Foundation (NSF). The Southern H-Alpha Sky Survey Atlas (SHASSA) is supported by the National Science Foundation. We thank the WHAM/SHASSA teams for making their surveys available and answering our queries. We also thank David Valls-Gabaud for verifying the calculation of the Gaunt factor.

REFERENCES

- Altenhoff W., Mezger P.G., Wendker H., Westerhout G., 1960, Veröff. Sternwarte Bonn, No 59, 48
- Baccigalupi C. et al., 2000, MNRAS, 318, 769
- Barnes, D.G. et al., 2001, MNRAS, 322, 486
- Bennett C.L. et al., 1992, ApJ, 396, L7
- Boumis P., Dickinson C., Meaburn J., Goudis C.D., Christopoulou P.E., López J.A., Bryce M., Redman M.P., 2001, MNRAS, 320, 61
- Burstein D., Heiles C., 1978, ApJ, 225, 40
- Davies R.D., 1963, Observatory, 83, 172
- Davies R.D., Watson R.A., Gutiérrez C.M., 1996, MNRAS, 278, 925
- de Oliveira-Costa A., Kogut A., Devlin M.J., Netterfield C.B., Page L.A., Wollack E.J., 1997, ApJ, 482, L17
- de Oliveira-Costa A., Tegmark M., Page L.M., Boughn S.P., 1998, ApJ, 509, L9
- de Oliveira-Costa A., Tegmark M., Gutiérrez C.M., Jones A.W., Davies R.D., Lasenby A.N., Rebolo R., Watson R.A., 1999, ApJ, 527, L9
- de Oliveira-Costa A. et al., 2000, ApJ, 542, L5
- de Oliveira-Costa A. et al., 2002, ApJ, 567, 363

- Dennison B., Simonetti J.H., Topsana G.A., 1998, *Publ. Astron. Soc. Aust.*, 15, 147
- Draine B.T., Lazarian A., 1998, *ApJ*, 494, L19
- Duncan A.R., Stewart R.T., Haynes R.F., Jones K.L., 1996, *MNRAS*, 280, 252
- Finkbeiner D.P., Schlegel D.J., Frank C., Heiles C., 2002, *ApJ*, 566, 898
- Gaustad J.E., McCullough P.R., Rosing W.R., Buren D.V., 2001, *PASP*, 113, 1326
- Gaylard M.J., 1984, *MNRAS*, 211, 149-153
- Górski K.M., Hivon E., Wandelt B.D., 1999, in *Proceedings of the MPA/ESO Cosmology Conference "Evolution of Large-Scale Structure"* eds. A.J. Banday, R.S. Sheth & L. Da Costa, 37
- Gum C.S., 1952, *Observatory*, 72, 151
- Haffner L.M., 1999, PhD Thesis, University of Wisconsin
- Haffner L.M., Reynolds R.J., Tuftte S.L., 1999, *ApJ*, 523, 223
- Halverson N.W. et al., 2002, *ApJ*, 568, 38
- Hanany S. et al., 2000, *ApJ*, 545, L5
- Hartmann D., Burton W.B., 1997, *Atlas of Galactic Neutral Hydrogen*, Cambridge University Press
- Haslam C.G.T., Salter C.J., Stoffel H., Wilson W., 1982, *A&AS*, 47, 1
- Hummer D.G., 1988, *ApJ*, 327, 477
- Hummer D.G., Storey P.J., 1987, *MNRAS*, 224, 801
- Jonas J.L., Baart E.E., Nicolson G.D., 1998, *MNRAS*, 297, 977
- Jones A.W., Davis R.J., Wilkinson A., Giardino G., Melhuish S.J., Asareh H., Davies R.D., Lasenby A.N., 2001, *MNRAS*, 327, 545
- Karzas W.J., Latter R., 1961, *ApJS*, 6, 167
- Kilborn V.A., 2002, *Seeing through the dust*, eds. R. Taylor, T. Landecker, T. Willis, *PASP*, in press
- Kogut A., Banday A.J., Bennett C.L., Górski K.M., Hinshaw G., Smoot G.F., Wright E.L., 1996, *ApJ*, 464, L5
- Large M.I., Mathewson D.S., Haslam C.G.T., 1961, *MNRAS*, 123, 123
- Leitch E.M., Readhead A.C.S., Pearson T.J., Myers S.T., 1997, *ApJ*, 486, L23
- Mauskopf P.D. et al., 2000, *ApJ*, 536, L59
- Meaburn J., 1965, *Nature*, 208, 575
- Meaburn J., 1967, *Zeits. Astrophysik.*, 65, 93
- Mezger P.G., Henderson A.P., 1967, *ApJ*, 147, 471
- O'Donnell J.E., 1994, *ApJ*, 422, 158
- Oster L., 1961, *Rev. Mod. Phys.*, 33, 525
- Osterbrock D.E., 1989, *Astrophysics of Gaseous Nebulae and Active Galactic Nuclei*, University Science Books, Mill Valley, California
- Padin S. et al., 2001, *ApJ*, 549, L1
- Panagia N., 1979, *Mem. Soc. Astron. Ital.*, 50, 79
- Parker Q.A., Phillipps S., 1998, *Publ. Astron. Soc. Aust.*, 15, 28
- Pengelly R.M., 1964, *MNRAS*, 127, 145
- Pottasch S.R., 1983, *Planetary Nebulae*, D. Reidel Publishing Company, Dordrecht, Holland, p. 285
- Reich P., Reich W., 1988, *A&AS*, 74, 7
- Reynolds R.J., 1985, *ApJ*, 294, 256
- Reynolds R.J., Ogden P.M., 1979, *ApJ*, 229, 942
- Reynolds R.J., Haffner L.M., 2002, *IAU Symposium 201*, eds. A.N. Lasenby, A. Wilkinson, *PASP*, in press
- Reynolds R.J., Tuftte S.L., Haffner L.M., Jaehnig K.P., Percival J.P., 1998, *Publ. Astron. Soc. Aust.*, 15, 14
- Reynosa E.M., Dubner G.M., 1997, *A&AS*, 123, 31
- Scheuer P.A.G., 1960, *MNRAS*, 120, 231
- Schlegel D.J., Finkbeiner D.P., Davis M., 1998, *ApJ*, 500, 525 (SFD98)
- Scott P.F. et al., 2002, submitted to *MNRAS*
- Shaver P.A., McGee R.X., Newton L.M., Danks A.C., Pottasch S.R., 1983, *MNRAS*, 204, 53
- Simonetti J.H., Dennison B., Topsana G.A., 1996, *ApJ*, 458, L1
- Sivan J.P., 1974, *A&AS*, 16, 163
- Taylor A.C. et al., 2002, submitted to *MNRAS*
- Valls-Gabaud D., 1998, *Publ. Astron. Soc. Aust.*, 15, 111
- Vielva P., Barreiro R.B., Hobson M.P., Martínez-González, E., Lasenby A.N., Sanz J.L., Toffolatti L., 2001, *MNRAS*, 328, 1
- Woermann B., Gaylard M.J., Otrupcek R., 2000, *MNRAS*, 315, 241
- Wollack E.J., Devlin M.J., Jarosik N., Netterfield C.B., Page L., Wilkinson D., 1997, *ApJ*, 476, 440